
Shortcut Detection with Variational Autoencoders

Nicolas M. Müller^{*1} Simon Roschmann^{*12} Shahbaz Khan^{*12} Philip Sperl¹ Konstantin Böttinger¹

Abstract

For real-world applications of machine learning (ML), it is essential that models make predictions based on well-generalizing features rather than spurious correlations in the data. The identification of such spurious correlations, also known as shortcuts, is a challenging problem and has so far been scarcely addressed. In this work, we present a novel approach to detect shortcuts in image and audio datasets by leveraging variational autoencoders (VAEs). The disentanglement of features in the latent space of VAEs allows us to discover correlations in datasets and semi-automatically evaluate them for ML shortcuts. We demonstrate the applicability of our method on several real-world datasets and identify shortcuts that have not been discovered before. Based on these findings, we also investigate the construction of shortcut adversarial examples.

1. Introduction

Machine learning (ML) addresses a wide range of real-world problems such as quality control (Yang et al., 2020), medical diagnosis (Rajpurkar et al., 2022) and facial recognition (Adjabi et al., 2020). However, transferring new ML technology from the lab to the real world is often difficult due to the limited capacity of ML models to generalize. Among the reasons for this limitation are shortcuts: features in data X that correlate only statistically with the target Y , but are inconsequential for the specific ML task.

Geirhos et al. (2020) define shortcuts as a certain group of decision rules learned by neural networks. Shortcuts perform well on training data and on independent and identically distributed (i.i.d.) test data but fail on out-of-distribution (o.o.d.) data. The learned solution deviates from the intended solution in the presence of a distribution shift.

Shortcut learning has been particularly evident in the medical field. A recent MIT technology report (Heaven, 2021) reveals that hundreds of tools were developed during the COVID-19 pandemic to diagnose the disease from chest X-rays, but none of them was found reliable enough for clinical use. The predictions of these models were often not based on the appearance of the lungs in the X-ray images. As the datasets were acquired from different sources for positive and negative cases, most of the models ended up learning the systematic differences in the data, e.g. the text fonts on the scans or the pose of the patient being scanned. Since the patients scanned while lying down were more likely to be seriously infected compared to those scanned while standing, the ML models wrongly learned to make a diagnosis based on a person’s position.

Shortcut learning can also be a cause of ethical concerns towards ML. Due to the existence of spurious correlations in the training data, ML models have been found to reinforce gender stereotypes (Bolukbasi et al., 2016; Dastin, 2018). Detecting shortcuts is thus a major challenge to ensure the reliability and fairness of artificial intelligence (AI). Only if a model correctly learns the semantically significant correlations during training instead of focusing on the prevalent spurious correlations in the data, can it be deployed for real-world applications.

Previous approaches (Zech et al., 2018; Singla & Feizi, 2021) for detecting shortcuts often rely on heatmaps and are thus limited to the identification of spatial shortcuts. We propose a novel method that is capable of identifying a variety of spurious features in images including background color, foreground color, object zoom level, and human facial characteristics. While other approaches (Lang et al., 2021; Atad et al., 2022) applied generative models such as GANs for counterfactual explanations, we are, to the best of our knowledge, the first to leverage variational autoencoders (VAEs) for shortcut detection.

We utilize a VAE to identify correlations between features of input X and target Y in datasets $D = (X, Y)$. We provide tools for visualization and statistical analysis on the latent space of the VAE which allow a human judge to reliably detect ML shortcuts as those correlations that are not meaningful to the task at hand.

^{*}Equal contribution ¹Fraunhofer AISEC, Germany ²Technical University of Munich, Germany. Correspondence to: Nicolas M. Müller <nicolas.mueller@aisec.fraunhofer.de>, Simon Roschmann <simon.roschmann@tum.de>, Shahbaz Khan <shahbaz.khan@tum.de>.

In summary, our contributions are:

- We introduce a VAE-based method to identify spurious correlations in datasets with minimal human supervision.
- We demonstrate the applicability of our approach by finding both artificially injected shortcuts as well as previously unknown, real-world shortcuts in publicly available image and audio datasets.
- We construct shortcut adversarial examples based on the spurious correlations identified by our method.

2. Related Work

Machine Learning Shortcuts. Geirhos et al. (2020) locate the origin of shortcuts in the data and the learning process of ML models. The inherent contextual bias in datasets provides opportunities for shortcuts. Natural image datasets contain spurious correlations between the target variable and the background (Xiao et al., 2020), the object poses (Alcorn et al., 2019) or other co-occurring distracting features (Kolesnikov & Lampert, 2016; Shetty et al., 2019). In discriminative learning, a model uses a combination of features to make a prediction. Following the “principle of least effort”, models tend to rely only on the most obvious features, which often correspond to shortcuts (Geirhos et al., 2020). For instance, convolutional neural networks (CNNs) trained on ImageNet were found to be biased towards the texture of the objects instead of their shapes (Geirhos et al., 2018). In another example, it was discovered that CNNs solely used the location of a single pixel to distinguish between object categories (Malhotra & Bowers, 2018).

Identification of Shortcuts. The identification of shortcuts in supervised machine learning is still in its infancy. Some of the existing Explainable AI (XAI) approaches have limited utility. Zech et al. (2018) use activation heatmaps to reveal the spurious features learned by CNNs trained on X-ray images. As outlined by Viviano et al. (2019), saliency maps can only explain spatial shortcuts, e.g. source tags on images (Lapuschkin et al., 2019), but fail to identify more complicated ones, e.g. people’s gender (Sagawa et al., 2019).

Singla and Feizi (2021) select the highest activations of neurons in the penultimate layer of a CNN classifier and back-project them onto the input images. The resulting heatmaps highlight the features in the image that maximize neural activations. Under human supervision, the highlighted regions, for a subset of images, are labelled as ‘core’ (part of the object definition) or ‘spurious’ (only co-occurring with the object). Using this labelled dataset, they train a classifier to automatically identify the core and spurious visual features for a larger dataset.

To diagnose shortcut learning, Geirhos et al. (2020) suggest performing o.o.d. generalization tests. Evaluating the model on o.o.d. real-world data in addition to the i.i.d. test set reveals whether a model is actually generalizing on the intended features or simply learning shortcuts from the training data.

Robustness against Shortcuts. To learn representations robust to spurious correlations, Zhang et al. (2022) propose a two-stage contrastive approach. The method first identifies training samples from the same class with different model predictions. Contrastive learning then ensures that the hidden representations for samples of the same class with initially different predictions become close to each other.

After training a classifier on shortcut-induced data, Kirichenko et al. (2022) retrain its last layer with Empirical Risk Minimization on a small dataset without spurious correlations. While the reweighting of the last layer reduces the model’s reliance on background and texture information, the requirement of a shortcut-free subset remains a limitation of this approach.

Proposed Improvements. Our approach overcomes a number of limitations from previous work. Most of the methods for explicit detection of shortcuts in a dataset are built on heatmaps and therefore limited to only identifying spatial shortcuts. Our method, on the other hand, identifies both spatial and non-spatial shortcuts as demonstrated in Section 4. Kirichenko et al. (2022) require a shortcut-free dataset for making a model robust against spurious correlations. Our method can serve as a preliminary step for this approach by identifying the shortcuts to be addressed.

3. Methodology

Let $D = (X, Y)$ be a dataset, where $X = \{x^{(i)} | x^{(i)} \in \mathbb{R}^{h \times w \times 3}\}_{i=1}^N$ are the images, $Y = \{y^{(i)} | y^{(i)} \in \{1, \dots, C\}\}_{i=1}^N$ are the corresponding targets and C is the number of classes. We train a VAE on such a dataset and perform statistical analysis on its latent space to identify feature-target correlations in the data. The visualization of traversal in the latent space allows a human judge to examine those correlations for shortcuts.

3.1. Variational Autoencoder

Our approach for shortcut detection is based on variational autoencoders (Kingma & Welling, 2013) (VAEs), which are probabilistic generative models that learn the underlying data distribution in an unsupervised manner. A VAE attempts to model the marginal likelihood of an observed variable x :

$$p_\theta(x) = \int p_\theta(z)p_\theta(x|z) dz \tag{1}$$

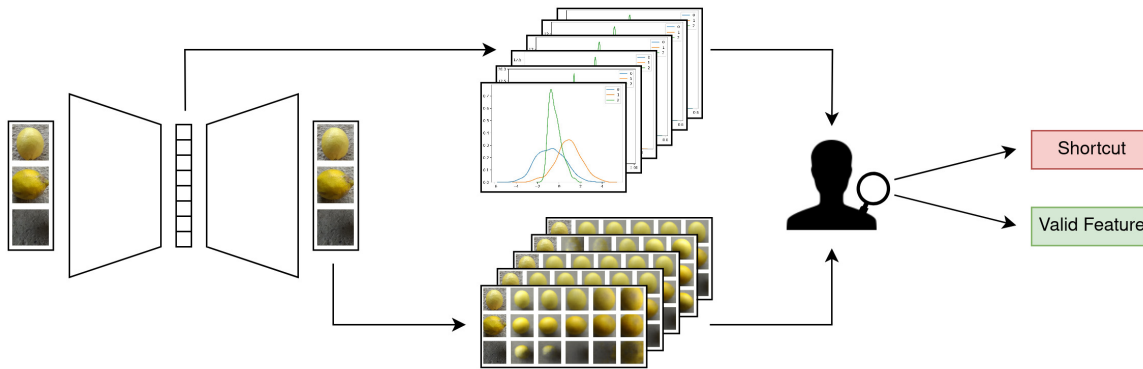


Figure 1. Shortcut Detection with a VAE. We first train a Beta-VAE on an image dataset containing potential shortcuts. The model discovers independent latent factors in the data and encodes them in its latent dimensions. Evaluating the distribution in the latent space (top) and the weights of a VAE classifier then yields a set of candidate dimensions with high predictiveness. The visualization of corresponding latent space traversals (bottom) enables a human judge to identify the meaning of these candidate dimensions and evaluate them for shortcuts/valid features.

The unobserved variable z lies in a latent space of dimensionality $d = \dim(z)$, $d \ll \dim(x)$. Each instance $x^{(i)}$ has a corresponding latent representation $z^{(i)}$.

The model assumes the prior over the latent variables to be a multivariate normal distribution $p_\theta(z) = \mathcal{N}(z; 0, I)$ resulting in independent latent factors $\{z_j\}_{j=1}^d$. The likelihood $p_\theta(x|z)$ is modelled as a multivariate Gaussian whose parameters are conditioned on $z \sim p_\theta(z)$ and computed using the VAE decoder. As outlined by Kingma and Welling (2013), the true posterior $p_\theta(z|x)$ is intractable and hence approximated with a variational distribution $q_\phi(z|x)$. This variational posterior is chosen to be a multivariate Gaussian

$$q_\phi(z|x^{(i)}) = \mathcal{N}(z; \mu^{(i)}, (\sigma^{(i)})^2 I) \quad (2)$$

whose mean $\mu^{(i)} \in \mathbb{R}^d$ and standard deviation $\sigma^{(i)} \in \mathbb{R}^d$ are obtained by forwarding $x^{(i)}$ through the VAE encoder. The objective function is composed of two terms. A Kullback-Leibler (KL) divergence term ensures that the variational posterior distribution remains close to the assumed prior distribution.

$$D_{KL}(q_\phi(z|x^{(i)})||p_\theta(z)) = -\frac{1}{2} \sum_{j=1}^d \left(1 + \log((\sigma_j^{(i)})^2) - (\sigma_j^{(i)})^2 - (\mu_j^{(i)})^2 \right) \quad (3)$$

A log-likelihood loss, on the other hand, helps to accurately reconstruct an input image $x^{(i)}$ from a sampled latent variable $z^{(i)} = \mu^{(i)} + \sigma^{(i)} \odot \epsilon$ where $\epsilon \sim \mathcal{N}(0, I)$. Thus the encoder and decoder are trained to maximize the following objective function:

$$\mathcal{L}(\theta, \phi; x^{(i)}) = -D_{KL}(q_\phi(z|x^{(i)})||p_\theta(z)) + \log p_\phi(x^{(i)}|z^{(i)}) \quad (4)$$

For modelling images, both the encoder and decoder of a VAE consist of CNNs.

Higgins et al. (2016) introduce the Beta-VAE to better learn independent latent factors. The authors propose to augment the vanilla VAE loss in Equation (4) by weighing the KL term with a hyperparameter β . Choosing $\beta > 1$ enables the model to learn a more efficient latent representation of the data with better disentangled dimensions.

3.2. Shortcut Detection with VAE

We train a Beta-VAE on an image dataset with potential shortcuts. The model discovers independent latent factors in a dataset and encodes them in its latent dimensions. Hence, each latent variable z_j of a trained Beta-VAE is likely to represent a descriptive property of the data, e.g. brightness, color, orientation, or shape (Higgins et al., 2016).

To establish feature-target correlations in the data, we measure how predictive each latent variable z_j is for each value of the target variable y (cf. Section 3.2.1). We perform a statistical analysis on the latent space of a VAE and assess the utility of its latent dimensions for linear classification. For latent variables z_j that show a strong correlation with the target variable y , we create visualizations that allow a human judge to easily decide whether the property encoded by z_j is a valid feature or a shortcut (see Section 3.2.2).

Our approach requires human inspection only for the candidate properties with the strongest feature-target correlations. In line with previous work, we argue that some form of human inspection will always be necessary to determine whether the model bases its decisions on relevant features or shortcuts.

In the following, we explain our method by applying it to

an exemplary dataset (the *Lemon Quality* dataset, cf. Section 4.2). In Section 4.3, we demonstrate that our approach is a reliable and easy way to identify shortcuts in various image and audio datasets.

3.2.1. IDENTIFICATION OF FEATURE-TARGET CORRELATIONS

Forwarding an image $x^{(i)}$ through the encoder of a trained Beta-VAE yields the parameters $\mu^{(i)}$ and $\sigma^{(i)}$ of the posterior $q_\phi(z|x^{(i)})$. The mean $\mu^{(i)}$ can be considered as the latent representation for $x^{(i)}$. We forward the entire dataset through the trained VAE, obtaining $\mu^{(i)}$ for all $i \in \{1, \dots, N\}$. We utilize these representations to determine the feature-target correlations in the data. We propose two different methods for this analysis.

Statistical Analysis on the Latent Space. For each latent dimension j and all target classes $c \in \{1, \dots, C\}$, we analyze the distributions $p(z_j|y=c)$, c.f. Figure 2. We are interested in finding those dimensions j where two different classes result in two highly disparate distribution estimates. This indicates that feature z_j is highly correlated with the target classes (a necessary, but not sufficient requirement for a shortcut). The separation between any two distributions is quantified in terms of the Wasserstein distance (Vaserstein, 1969) between them. We hypothesize that the maximum pairwise Wasserstein distance (MPWD) for a particular dimension represents its capability to separate classes. The k dimensions with the largest MPWD are selected as candidates for shortcut evaluation.

Additionally, we visualize the distributions for a particular latent dimension using Kernel Density Estimation (KDE) (Rosenblatt, 1956; Parzen, 1962). For each latent dimension j and class $c \in \{1, \dots, C\}$, we estimate $p(z_j|y=c)$ over the training data $\{x^{(i)}|y^{(i)}=c\}_{i=1}^N$:

$$p(z_j|y=c) = \frac{1}{hK_c} \sum_{n=1}^{|K_c|} \frac{1}{\sqrt{2\pi}} \exp\left(-\frac{(z_j - \mu_j^{(n)})^2}{2h^2}\right) \quad (5)$$

where h is the bandwidth parameter and $K_c = \{i|y^{(i)}=c\}$ are the indices of all images belonging to class c . Figure 2 illustrates this approach for the latent dimension 2 of a Beta-VAE trained on the *Lemon Quality* dataset.

Classification with VAE Encoder. Another approach to understanding the correlation between z_j and y is to employ a classifier to predict y given z . We pick the encoder of our trained Beta-VAE and append a fully connected layer. After freezing the encoder backbone, we optimize its dense classification head. The weights in the last layer of this model denote the correlation between the latent dimensions and the target classes. For a dense classification head $h(z) \rightarrow y$,

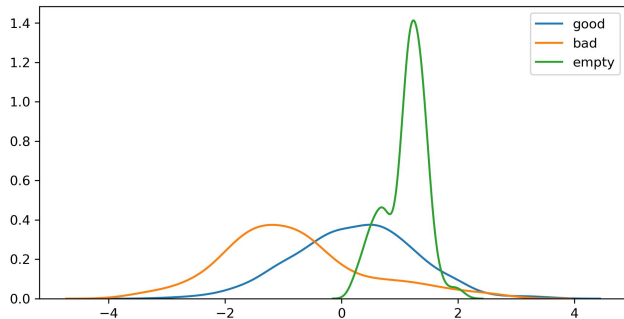


Figure 2. Statistical analysis on the latent space. The distributions correspond to latent dimension 2 of a Beta-VAE trained on the *Lemon Quality* dataset. The large distance between the density estimates for each class indicates a high correlation between feature z_2 and the target classes. While negative values are mostly associated with the class ‘bad quality’, positive values are associated with ‘good quality’.

we define the predictiveness of feature z_j as

$$\text{pred}(z_j) = \sum_c |\theta_{jc}| \quad (6)$$

where θ_{jc} is the weight of the neuron in h which maps input z_j to output $h(z_j)_c$. We select the top k dimensions with the largest predictiveness as candidates for shortcut evaluation.

3.2.2. EVALUATION OF FEATURE-TARGET CORRELATIONS FOR SHORTCUTS

After identifying the most predictive features in the latent space, we can now evaluate them for shortcuts. To facilitate the distinction between valid and spurious correlations, we provide a human judge with visualizations that convey the meaning of the features.

Visualizing z_j via Latent Space Traversal. The first approach to understanding high-level features encoded in a latent dimension z_j is to visualize the effect of traversal in that dimension using the trained Beta-VAE. Given an instance $x^{(i)}$, we obtain $z^{(i)} = \mu^{(i)}$ from the encoder and then visualize the decoder output $Dec(z^{(i)} + \lambda)$. The linear interpolation in the latent space is specified by λ where $\lambda_j \in [z_j^{min}, z_j^{max}]$, $z_j^{min} = \min(\{z_j^{(i)}\}_{i=1}^N)$, $z_j^{max} = \max(\{z_j^{(i)}\}_{i=1}^N)$ and $\lambda_k = 0$ for $k \neq j$. This helps us to understand whether the latent variable z_j encodes a useful feature or a shortcut. Figure 3 illustrates the latent traversal for the *Lemon Quality* dataset.

Visualizing Images for Extreme z_j . To validate the meaning attributed to z_j , we compute the embeddings $z_j^{(i)}$ for all the instances $x^{(i)}$ in the dataset, and identify those instances which minimize or maximize z_j . Particularly, we perform $\arg \text{sort}_i(\{z_j^{(i)}\}_{i=1}^N)$ for every dimension j in the

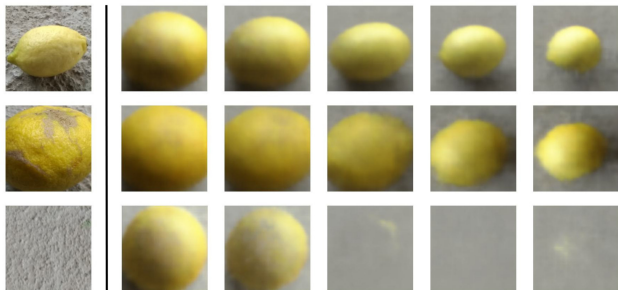


Figure 3. Latent space traversal. The first column shows examples for the three classes (‘good quality’, ‘bad quality’, ‘empty background’) from the *Lemon Quality* dataset. We vary the value of dimension 2 in the latent space from $z_2^{min} = -3.75$ (second column) to $z_2^{max} = 3.64$ (rightmost column) while keeping the values of the other dimensions fixed. Decoding the new latent representation reveals that dimension 2 encodes the zoom level of the images. While close-up shots (on the left) correlate with class ‘bad quality’, distant shots (on the right) correlate with class ‘good quality’.

latent space and display the input images $x^{(i)}$ corresponding to the first l and the last l indices of the sorted values. Figure 4 depicts $l = 27$ images of the *Lemon Quality* dataset with minimum and maximum values in latent dimension 2.

3.2.3. ON THE NECESSITY OF HUMAN JUDGES

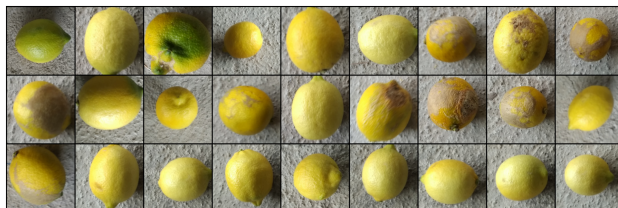
Our method requires a human judge to evaluate if the information encoded by the latent variable z_j constitutes a feature or a shortcut. We argue that human interventions are inevitable for ML-based shortcut detection (Zech et al., 2018; Geirhos et al., 2020; Singla & Feizi, 2021). ML models learn relations between input and output based on statistics alone. Unlike humans, they are hardly equipped with prior knowledge of the real world beyond the given dataset and the specified task. However, this prior knowledge may be necessary to evaluate whether a correlation is valid or spurious. Therefore, to assess the candidate feature-target correlations identified by our model, we need a human judge in the last step of our approach. This human supervision is limited to inferring the meaning of a latent dimension from the visualization of its latent traversal.

4. Evaluation

We perform shortcut detection with our proposed method on synthetic and real-world datasets. Not only does our method rediscover known shortcuts in these datasets, it also reveals a previously unknown shortcut in a real-world dataset. Additionally, we exploit the knowledge about these spurious correlations to generate shortcut adversarial examples.



(a) Inputs from the *Lemon Quality* dataset which minimize z_2 .



(b) Inputs from the *Lemon Quality* dataset which maximize z_2 .

Figure 4. Real-world images from the training dataset that correspond to the minimum and maximum encoded values in latent dimension 2. While bad-quality lemons are mostly captured as close-up shots, good-quality lemons are photographed from a distance.

4.1. Experimental Setup

To obtain a low-dimensional latent representation, we use a Beta-VAE (cf. Section 3.1) with $dim(z) \in \{10, 32\}$ depending on the data. For our encoder, we employ a ResNet (He et al., 2016) backbone pretrained on the ImageNet (Russakovsky et al., 2015) dataset. We append two separate linear layers for predicting the parameters μ and σ of the posterior distribution. The decoder of our model consists of 5 hidden layers, each applying transposed convolutions with padding 1, stride 2, and kernel size 3. The channel dimensions of the hidden layers in the decoder are chosen as follows: 512, 256, 128, 64, and 32. We apply ReLU activation and batch normalization in the hidden layers and Sigmoid activation in the output layer.

Our model is trained using the Adam (Kingma & Ba, 2014) optimizer with a learning rate of 0.001 to optimize the loss described in Equation (4). We train the model with early stopping (patience of 10 epochs) and a batch size of 32. Since β determines the tradeoff between reconstruction and sampling quality, we perform hyperparameter tuning on β for each dataset. Details are provided in the Appendix. The generation of high-quality samples indicates that our model is able to discover meaningful latent factors which is a prerequisite for shortcut detection.

While our model can operate on varying input sizes, we use images of size 128×128 in our experiments. We do not perform any data augmentation so as to retain the original characteristics of the input data including any shortcut.

Table 1. Shortcut detection results. For every dataset, we denote the dimension of a trained VAE which encodes a spuriously correlated attribute. They are picked from a set of candidate dimensions shortlisted based on how predictive (cf. Section 3.2.1) they are in relation to all dimensions. The semantic meaning encoded by these candidate dimensions is revealed with a traversal in the latent space (cf. Section 3.2.2).

| Dataset | Spurious Dimension | Spurious Attribute | MPWD | Predictiveness |
|---------------|--------------------|--------------------|------|----------------|
| ASVspoof | 30 | Leading silence | 2/32 | 2/32 |
| CelebA | 26 | Gender | 3/32 | 3/32 |
| Colored MNIST | 14 | Color | 1/32 | 1/32 |
| COVID-19 | 1 | Patient’s position | 1/32 | 2/32 |
| Lemon Quality | 2 | Zoom level | 1/10 | 2/10 |
| Waterbirds | 1 | Background | 2/32 | 3/32 |

To estimate the predictiveness of latent features, we append a linear layer to the frozen encoder of a trained Beta-VAE. The resulting classifier with cross-entropy loss is trained with early stopping (patience of 10 epochs), the Adam optimizer and a learning rate of 0.001 on batches of size 32.

We ran all experiments on an Nvidia Titan X 12GB GPU.

4.2. Datasets

We evaluate our approach on datasets with artificially introduced shortcuts to demonstrate its ability to identify spurious correlations. Our method can also be applied to real-world datasets to reveal previously unknown shortcuts. We perform a train-val-test split in the ratio 80:10:10 on each dataset unless specified differently.

Waterbirds. Sagawa et al. (2019) extract birds from the Caltech-UCSD Birds-200-2011 dataset (Wah et al., 2011) and combine them with background images from the Places dataset (Zhou et al., 2017). As a result, 95% of the water birds appear on a water background while 95% of the land birds appear on a land background. Since this spurious correlation is only introduced in the train set of the *Waterbirds* dataset consisting of 4,795 samples, we use the same to create the train-val-test splits for our experiments.

Colored MNIST. Arjovsky et al. (2019) inject color as a spurious attribute into the MNIST (LeCun et al., 2010) dataset. Following this idea, Zhang et al. (2022) create a colored MNIST dataset consisting of five subsets with five associated colors. A fraction p_{corr} of the training samples are assigned colors based on the group they belong to. The remaining samples are assigned a random color. We follow the color assignment in (Zhang et al., 2022) and choose $p_{corr} = 0.995$ for coloring the 70,000 MNIST samples.

CelebA. The CelebFaces Attributes Dataset (Liu et al., 2015) contains 202,599 images of celebrities, each annotated with 40 facial attributes. Sagawa et al. (2019) train a classifier to identify the hair color of the celebrities and discover that the target classes (blond, dark) are spuriously

correlated with the gender (male, female). We stick to the setup specified in (Sagawa et al., 2019) with the official train-val-test splits of the *CelebA* dataset.

Lemon Quality. To demonstrate the detection of shortcuts in quality control, we apply our method on the *Lemon Quality* dataset (Köroğlu, 2020). The dataset consists of 2,533 images labelled with one of three classes, namely ‘good quality’, ‘bad quality’, and ‘empty background’.

COVID-19. Following (Brunese et al., 2020; Ghoshal & Tucker, 2020; Hemdan et al., 2020; Ozturk et al., 2020; DeGrave et al., 2021), we obtain a dataset with 112,528 samples for COVID-19 detection by combining COVID-19-positive radiographs from the GitHub-COVID repository (Cohen et al., 2020) and COVID-19-negative radiographs from the ChestX-ray14 repository (Wang et al., 2017).

ASVspoof. The ASVspoof 2019 Challenge Dataset (Wang et al., 2020) is used to train and benchmark systems for the detection of spoofed audio and audio deepfakes. Müller et al. (2021) observe that the length of the silence at the beginning of an audio sample differs significantly between benign and malicious data. Previous deepfake detection models have exploited this shortcut. We chose a subset of the training data (benign audio and attack A01), which results in a binary classification dataset comprising 6,380 samples. We transform the audio samples to CQT spectrograms (Schörkhuber & Klapuri, 2010), and obtain a frequency-domain representation with 257 logarithmically spaced frequency bins, capturing up to 8 kHz (Nyquist frequency given the input is 16 kHz).

4.3. Results

For every dataset under examination, we present a feature that highly correlates with the targets but is not relevant for the actual task and thus considered a shortcut. While the particular dimension representing such a feature can vary between different training runs, any VAE trained with well-chosen hyperparameters should be able to encode the feature in one of its latent dimensions. Table 1 summarizes

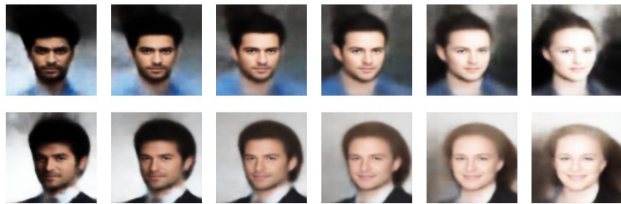


Figure 5. Evaluation of our method on the *CelebA* dataset. Latent traversal reveals the spurious correlation between gender and hair color through the transition from males (left) to females (right).

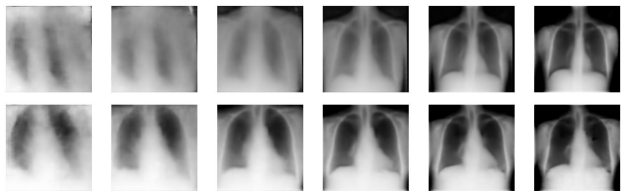


Figure 6. Evaluation of our method on the *COVID-19* dataset. The spurious correlation between the position of the patient’s chest in the X-ray images and the diagnosis becomes evident through latent space traversal. Patients with ‘covid’ appear closer to the scanner (left) while patients with ‘no covid’ appear further away such that black background on the top and bottom sides is visible (right).

our results. The MPWD and the predictiveness of a spurious dimension are reported relative to the other latent dimensions. Across all experiments, we conclude that a human judge has to review only the top $k = 3$ latent dimensions with the highest MPWD and predictiveness to identify a shortcut if present in the data. Both scores lead to a similar set of candidate dimensions for shortcut evaluation.

Our approach correctly identifies the known shortcut in the *CelebA* dataset. The statistical analysis on the latent space of a trained VAE shows that its latent variable z_{26} has a high MPWD (among top 3) and a high predictiveness $pred(z_{26})$ (among top 3). The latent traversal illustrated in Figure 5 reveals that the latent variable z_{26} encodes the gender of a person. Similarly, we detect the color shortcut in the *Colored MNIST* dataset and the background shortcut in the *Waterbirds* dataset. Illustrations of the respective latent traversals can be found in the Appendix.

To the best of our knowledge, we are the first to identify the existence of a shortcut in the *Lemon Quality* dataset. As depicted in Figure 3, our method reveals the correlation between lemon quality and zoom level. The good-quality lemons are mostly photographed from a distance. The bad-quality lemons, on the other hand, are mostly captured in close-up shots. The identification of the position shortcut in the *COVID-19* dataset is illustrated in Figure 6 and confirms the findings of DeGrave et al. (2021). We make a step towards the generalization of our method to other domains

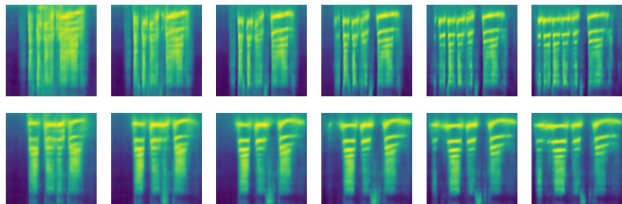


Figure 7. Evaluation of our method on the *ASVspoof* dataset. Latent traversal reaffirms the known spurious correlation between the leading silence in the audio and the target class. Leading silence (left) in the spectrogram is an indicator of benign audio samples while no leading silence (right) is common in spoofs.

by identifying shortcuts in spectrograms from the *ASVspoof* dataset. Figure 7 exhibits the latent traversal for the spurious silence feature in the *ASVspoof* dataset.

A perfect disentanglement in the latent space facilitates the identification of the semantic meaning of a dimension. However, the existence of shortcuts in a dataset makes it difficult for a model to fully separate the factors of variation. Thus, we sometimes observe (see Figure 6) that the change of a spurious attribute (e.g. position) coincides with the change of the main distinguishing factor (e.g. lung appearance).

4.4. Shortcut Adversarial Examples

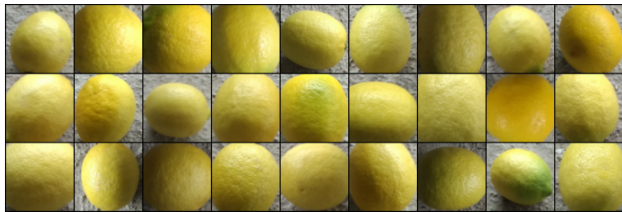
In addition to identifying the underlying shortcuts in a given dataset, our method enables to create shortcut adversarial examples. Adversarial examples are specifically crafted data points $\hat{x} = x + \delta$ that are recognized by humans as their true class y , but classified by a model f as a different class $t \neq y$. Such examples can for instance be found by solving the following minimization problem (Szegedy et al., 2013)

$$\arg \min_{\delta} L(f(x + \delta), t) + \lambda \|\delta\|_2^2 \quad (7)$$

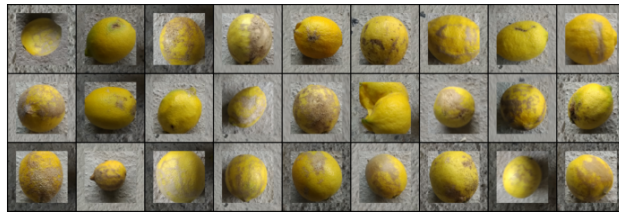
where L is the training loss and λ constrains the magnitude of the perturbation δ . Equation (7) is usually solved using gradient-based optimization, which is computationally expensive and either requires access to the model parameters or necessitates the use of surrogate models, e.g. in transfer-based attacks (Chakraborty et al., 2018).

The existence of shortcuts paves the way for a new approach of generating adversarial examples. Shortcut adversarial examples can be created by modifying an original image such that it carries a shortcut feature that the model associates with another class. This modification of the image, however, does not change its class as perceived by humans.

For example, by cropping the centre of an image showing a good-quality lemon, we mimic a close-up shot of the fruit. Since the model associates close-up shots with bad-quality lemons, it classifies the modified image as ‘bad quality’.



(a) Cropping the center regions of good-quality images to mimic a close up shot.



(b) Padding bad-quality images with empty background pixels to mimic a distant shot.

Figure 8. Shortcut adversarial examples for the *Lemon quality* dataset generated by exploiting the spurious correlation between the zoom-level of the image and the target labels. The good quality lemons in Figure 8a tend to be misclassified by the model as ‘bad quality’. Similarly, the bad-quality lemons in Figure 8b with the mimicked zoomed-out levels are now likely to be misclassified as ‘good quality’.

Similarly, we mimic a distant shot by padding images of bad-quality lemons with empty background pixels. Figure 8 illustrates the creation of shortcut adversarial examples for the *Lemon Quality* dataset.

Based on the shortcuts discovered, we only perform a simple image manipulation instead of iteratively computing gradients for the optimization of Equation (7). Furthermore, our method does not require access to the target model parameters and is computationally less expensive than established proxy attacks (Brendel et al., 2017; Chen et al., 2017; Ilyas et al., 2018).

Shortcut adversarial examples are related to backdoor attacks (Li et al., 2022) where an adversary injects a trigger into the training dataset to cause an ML model to learn certain adversarial patterns. The model under attack behaves correctly on benign test samples while its predictions turn faulty when the embedded backdoor is triggered. Shortcuts can be seen as backdoors inherent to a given dataset. We do not perform backdoor attacks as we do not inject shortcuts into the training dataset. Instead, we exploit their natural occurrence in the data to generate adversarial examples on which a model is likely to fail at test time.

Our shortcut adversarial examples are effective and model agnostic. We employ a CNN classifier comprising 5 convolutional layers with 32, 64, 128, 256, and 512 filters of size 3×3 . Each of these layers is followed by ReLU activation and max pooling. When trained on the *Lemon Quality* train set, this model reaches an overall accuracy of 98.4% on the unperturbed *Lemon Quality* test set. Applying the model on shortcut adversarial examples created from this test set decreases the test accuracy for good lemons from 98.3% to 65% and for bad lemons from 97.7% to 86.6%. This is because the classifier learns to rely on the spurious correlation between the zoom level and target class for its prediction.

4.5. Limitations

A VAE used for shortcut detection is required to learn meaningful, disentangled factors in its latent space. The Beta-VAE employed in our method can encode a disentangled representation (Higgins et al., 2016) only if the underlying factors of a dataset are independent. Our method relies on this assumption.

Through our experiments, we discovered that a Beta-VAE with ResNet encoder lacks the ability to model datasets with a large number of visually diverse classes such as ImageNet (Russakovsky et al., 2015). More powerful models like NVAE (Vahdat & Kautz, 2020) could enhance the modelling and sampling quality on such datasets. However, the size of their latent space and the hierarchical entanglement of features limits their usage in shortcut detection.

Finally, we note that VAEs are sensitive to the choice of hyperparameters. The number of latent dimensions should be in accordance with the number of factors of variation in a dataset. The weights assigned to the KL divergence and reconstruction loss are vital for the overall performance of a VAE and thus have to be finetuned for every dataset.

5. Conclusion

In this paper, we introduce a novel approach to detect spurious correlations in machine learning datasets. Our method utilizes a VAE to discover meaningful features in a given dataset and enables a human judge to identify shortcuts effortlessly. We evaluate our approach on image and audio datasets and successfully reveal inherent shortcuts. We further demonstrate how the knowledge of these spurious correlations can be exploited to generate shortcut adversarial examples.

We hope that our work inspires researchers to explore the potential of VAEs in the field of shortcut learning. It would be interesting to see if our method can be extended to other domains.

References

- Adjabi, I., Ouahabi, A., Benzaoui, A., and Taleb-Ahmed, A. Past, present, and future of face recognition: A review. *Electronics*, 9(8):1188, 2020.
- Alcorn, M. A., Li, Q., Gong, Z., Wang, C., Mai, L., Ku, W.-S., and Nguyen, A. Strike (with) a pose: Neural networks are easily fooled by strange poses of familiar objects. In *Proceedings of the IEEE/CVF Conference on Computer Vision and Pattern Recognition*, pp. 4845–4854, 2019.
- Arjovsky, M., Bottou, L., Gulrajani, I., and Lopez-Paz, D. Invariant risk minimization. *arXiv preprint arXiv:1907.02893*, 2019.
- Atad, M., Dmytrenko, V., Li, Y., Zhang, X., Keicher, M., Kirschke, J., Wiestler, B., Khakzar, A., and Navab, N. Chexplaining in style: Counterfactual explanations for chest x-rays using stylegan. *arXiv preprint arXiv:2207.07553*, 2022.
- Bolukbasi, T., Chang, K.-W., Zou, J. Y., Saligrama, V., and Kalai, A. T. Man is to computer programmer as woman is to homemaker? debiasing word embeddings. *Advances in neural information processing systems*, 29, 2016.
- Brendel, W., Rauber, J., and Bethge, M. Decision-based adversarial attacks: Reliable attacks against black-box machine learning models. *arXiv preprint arXiv:1712.04248*, 2017.
- Brunese, L., Mercaldo, F., Reginelli, A., and Santone, A. Explainable deep learning for pulmonary disease and coronavirus covid-19 detection from x-rays. *Computer Methods and Programs in Biomedicine*, 196:105608, 2020.
- Chakraborty, A., Alam, M., Dey, V., Chattopadhyay, A., and Mukhopadhyay, D. Adversarial attacks and defences: A survey. *arXiv preprint arXiv:1810.00069*, 2018.
- Chen, P.-Y., Zhang, H., Sharma, Y., Yi, J., and Hsieh, C.-J. Zoo: Zeroth order optimization based black-box attacks to deep neural networks without training substitute models. In *Proceedings of the 10th ACM workshop on artificial intelligence and security*, pp. 15–26, 2017.
- Cohen, J. P., Morrison, P., and Dao, L. Covid-19 image data collection. *arXiv preprint 2003.11597*, 2020. URL <https://github.com/ieee8023/covid-chestxray-dataset>.
- Dastin, J. Amazon scraps secret ai recruiting tool that showed bias against women. <https://www.reuters.com/article/us-amazon-com-jobs-automation-insight/amazon-scraps-secret-ai-recruiting-tool-that-showed-bias-against-women-idUSKCN1MK08G/>, 11 2018. (Accessed on 12/26/2022).
- DeGrave, A. J., Janizek, J. D., and Lee, S.-I. Ai for radiographic covid-19 detection selects shortcuts over signal. *Nature Machine Intelligence*, 3(7):610–619, 2021.
- Geirhos, R., Rubisch, P., Michaelis, C., Bethge, M., Wichmann, F. A., and Brendel, W. Imagenet-trained cnns are biased towards texture; increasing shape bias improves accuracy and robustness. *arXiv preprint arXiv:1811.12231*, 2018.
- Geirhos, R., Jacobsen, J.-H., Michaelis, C., Zemel, R., Brendel, W., Bethge, M., and Wichmann, F. A. Shortcut learning in deep neural networks. *Nature Machine Intelligence*, 2(11):665–673, 2020.
- Ghoshal, B. and Tucker, A. Estimating uncertainty and interpretability in deep learning for coronavirus (covid-19) detection. *arXiv preprint arXiv:2003.10769*, 2020.
- He, K., Zhang, X., Ren, S., and Sun, J. Deep residual learning for image recognition. In *Proceedings of the IEEE conference on computer vision and pattern recognition*, pp. 770–778, 2016.
- Heaven, W. D. Hundreds of ai tools have been built to catch covid. none of them helped. mit technology review. <https://www.technologyreview.com/2021/07/30/1030329/machine-learning-ai-failed-covid-hospital-diagnosis-pandemic/>, 07 2021. (Accessed on 11/13/2022).
- Hemdan, E. E.-D., Shouman, M. A., and Karar, M. E. Covidx-net: A framework of deep learning classifiers to diagnose covid-19 in x-ray images. *arXiv preprint arXiv:2003.11055*, 2020.
- Higgins, I., Matthey, L., Pal, A., Burgess, C., Glorot, X., Botvinick, M., Mohamed, S., and Lerchner, A. beta-vae: Learning basic visual concepts with a constrained variational framework. *Openreview*, 2016.
- Ilyas, A., Engstrom, L., Athalye, A., and Lin, J. Black-box adversarial attacks with limited queries and information. In *International Conference on Machine Learning*, pp. 2137–2146. PMLR, 2018.
- Kingma, D. P. and Ba, J. Adam: A method for stochastic optimization. *arXiv preprint arXiv:1412.6980*, 2014.
- Kingma, D. P. and Welling, M. Auto-encoding variational bayes. *arXiv preprint arXiv:1312.6114*, 2013.
- Kirichenko, P., Izmailov, P., and Wilson, A. G. Last layer re-training is sufficient for robustness to spurious correlations. *arXiv preprint arXiv:2204.02937*, 2022.
- Kolesnikov, A. and Lampert, C. H. Improving weakly-supervised object localization by micro-annotation. *arXiv preprint arXiv:1605.05538*, 2016.

- Köroğlu, Y. E. Lemon quality dataset. <https://www.kaggle.com/datasets/yusufemir/lemon-quality-dataset>, 2020. (Accessed on 11/13/2022).
- Lang, O., Gandelsman, Y., Yarom, M., Wald, Y., Elidan, G., Hassidim, A., Freeman, W. T., Isola, P., Globerson, A., Irani, M., et al. Explaining in style: Training a gan to explain a classifier in stylespace. In *Proceedings of the IEEE/CVF International Conference on Computer Vision*, pp. 693–702, 2021.
- Lapuschkin, S., Wäldchen, S., Binder, A., Montavon, G., Samek, W., and Müller, K.-R. Unmasking clever hans predictors and assessing what machines really learn. *Nature communications*, 10(1):1–8, 2019.
- LeCun, Y., Cortes, C., and Burges, C. Mnist handwritten digit database. *ATT Labs [Online]*. Available: <http://yann.lecun.com/exdb/mnist>, 2, 2010.
- Li, Y., Jiang, Y., Li, Z., and Xia, S.-T. Backdoor learning: A survey. *IEEE Transactions on Neural Networks and Learning Systems*, 2022.
- Liu, Z., Luo, P., Wang, X., and Tang, X. Deep learning face attributes in the wild. In *Proceedings of the IEEE international conference on computer vision*, pp. 3730–3738, 2015.
- Malhotra, G. and Bowers, J. What a difference a pixel makes: an empirical examination of features used by cnns for categorisation. *Openreview*, 2018.
- Müller, N. M., Dieckmann, F., Czempin, P., Canals, R., Böttinger, K., and Williams, J. Speech is silver, silence is golden: What do asvspoof-trained models really learn? *arXiv preprint arXiv:2106.12914*, 2021.
- Ozturk, T., Talo, M., Yildirim, E. A., Baloglu, U. B., Yildirim, O., and Acharya, U. R. Automated detection of covid-19 cases using deep neural networks with x-ray images. *Computers in biology and medicine*, 121:103792, 2020.
- Parzen, E. On estimation of a probability density function and mode. *The annals of mathematical statistics*, 33(3): 1065–1076, 1962.
- Rajpurkar, P., Chen, E., Banerjee, O., and Topol, E. J. Ai in health and medicine. *Nature Medicine*, 28(1):31–38, 2022.
- Rosenblatt, M. Remarks on some nonparametric estimates of a density function. *The annals of mathematical statistics*, pp. 832–837, 1956.
- Russakovsky, O., Deng, J., Su, H., Krause, J., Satheesh, S., Ma, S., Huang, Z., Karpathy, A., Khosla, A., Bernstein, M., et al. Imagenet large scale visual recognition challenge. *International journal of computer vision*, 115(3): 211–252, 2015.
- Sagawa, S., Koh, P. W., Hashimoto, T. B., and Liang, P. Distributionally robust neural networks for group shifts: On the importance of regularization for worst-case generalization. *arXiv preprint arXiv:1911.08731*, 2019.
- Schörkhuber, C. and Klapuri, A. Constant-q transform toolbox for music processing. In *7th sound and music computing conference, Barcelona, Spain*, pp. 3–64, 2010.
- Shetty, R., Schiele, B., and Fritz, M. Not using the car to see the sidewalk—quantifying and controlling the effects of context in classification and segmentation. In *Proceedings of the IEEE/CVF Conference on Computer Vision and Pattern Recognition*, pp. 8218–8226, 2019.
- Singla, S. and Feizi, S. Causal imagenet: How to discover spurious features in deep learning? *arXiv preprint arXiv:2110.04301*, 2021.
- Szegedy, C., Zaremba, W., Sutskever, I., Bruna, J., Erhan, D., Goodfellow, I., and Fergus, R. Intriguing properties of neural networks. *arXiv preprint arXiv:1312.6199*, 2013.
- Vahdat, A. and Kautz, J. Nvae: A deep hierarchical variational autoencoder. *Advances in Neural Information Processing Systems*, 33:19667–19679, 2020.
- Vaserstein, L. N. Markov processes over denumerable products of spaces, describing large systems of automata. *Problemy Peredachi Informatsii*, 5(3):64–72, 1969.
- Viviano, J. D., Simpson, B., Dutil, F., Bengio, Y., and Cohen, J. P. Saliency is a possible red herring when diagnosing poor generalization. *arXiv preprint arXiv:1910.00199*, 2019.
- Wah, C., Branson, S., Welinder, P., Perona, P., and Belongie, S. The caltech-ucsd birds-200-2011 dataset. *Caltech Online Library*, 2011.
- Wang, X., Peng, Y., Lu, L., Lu, Z., Bagheri, M., and Summers, R. M. Chestx-ray8: Hospital-scale chest x-ray database and benchmarks on weakly-supervised classification and localization of common thorax diseases. In *Proceedings of the IEEE conference on computer vision and pattern recognition*, pp. 2097–2106, 2017.
- Wang, X., Yamagishi, J., Todisco, M., Delgado, H., Nautsch, A., Evans, N., Sahidullah, M., Vestman, V., Kinnunen, T., Lee, K. A., et al. Asvspoof 2019: A large-scale public database of synthesized, converted and replayed speech. *Computer Speech & Language*, 64:101114, 2020.

- Xiao, K., Engstrom, L., Ilyas, A., and Madry, A. Noise or signal: The role of image backgrounds in object recognition. *arXiv preprint arXiv:2006.09994*, 2020.
- Yang, J., Li, S., Wang, Z., Dong, H., Wang, J., and Tang, S. Using deep learning to detect defects in manufacturing: a comprehensive survey and current challenges. *Materials*, 13(24):5755, 2020.
- Zech, J. R., Badgeley, M. A., Liu, M., Costa, A. B., Titano, J. J., and Oermann, E. K. Confounding variables can degrade generalization performance of radiological deep learning models. *arXiv preprint arXiv:1807.00431*, 2018.
- Zhang, M., Sohoni, N. S., Zhang, H. R., Finn, C., and Ré, C. Correct-n-contrast: A contrastive approach for improving robustness to spurious correlations. *arXiv preprint arXiv:2203.01517*, 2022.
- Zhou, B., Lapedriza, A., Khosla, A., Oliva, A., and Torralba, A. Places: A 10 million image database for scene recognition. *IEEE transactions on pattern analysis and machine intelligence*, 40(6):1452–1464, 2017.

A. Hyperparameter Tuning of Beta-VAE

Following Higgins et al. (2016), we tune the hyperparameters $\dim(z)$ and β of the Beta-VAE for every dataset. To achieve maximum disentanglement, the number of latent dimensions should match the number of factors of variation in a dataset. This number is usually not known a priori. Choosing a latent space of too high dimensionality leads to a lot of uninformative dimensions with low variance. A latent space of too few latent dimensions, on the other hand, leads to entangled representations of features in the latent space. Therefore, it is necessary to identify the optimal number of latent dimensions to achieve maximally disentangled factors, ideally one in each dimension.

To obtain the best combination of β and $\dim(z)$ for a given dataset, we first train a Beta-VAE with $\beta = 1$ and $\dim(z) = 32$ on all datasets. We then compare the variance of the distribution in each dimension to that of a Gaussian prior. In the presence of dimensions with relatively low variance, we reduce the number of latent dimensions. Once we find a Beta-VAE with consistently informative dimensions, i.e. with the variance comparable to the prior, we fix $\dim(z)$ and focus on fine-tuning β . As outlined by Higgins et al. (2016), for relatively low values of β , the VAE learns an entangled latent representation since the capacity in the latent space is too high. On the other hand, for relatively high values of β , the capacity in the latent space becomes too low. The VAE performs a low-rank projection of the true data generative factors and again learns an entangled latent representation. This renders some of the latent dimensions uninformative.

We find the highest possible β for which all dimensions of the VAE remain informative with a variance close to the prior. In line with the findings of Higgins et al. (2016), $\beta > 1$ is required for all datasets to achieve good disentanglement (see Table 2).

Table 2. Beta-VAE hyperparameters

| Dataset | $\dim(z)$ | β |
|---------------|-----------|---------|
| ASVspoof | 32 | 1.25 |
| CelebA | 32 | 10.0 |
| Colored MNIST | 32 | 2.5 |
| COVID-19 | 32 | 1.5 |
| Lemon Quality | 10 | 3.0 |
| Waterbirds | 32 | 1.75 |

B. Evaluation

We provide illustrations of the latent space traversal for the *Waterbirds* and *Colored MNIST* dataset.

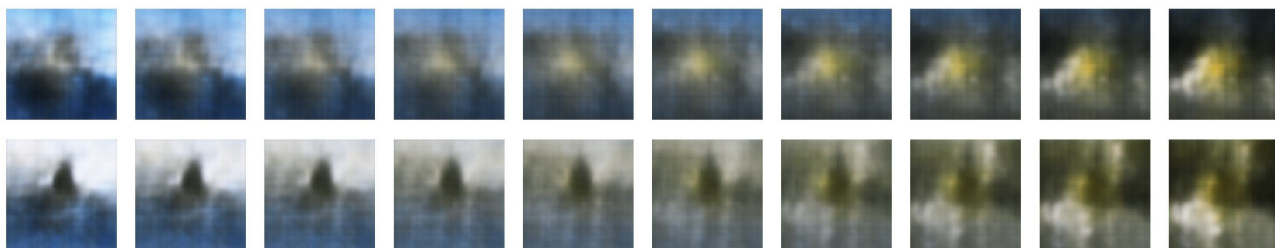


Figure 9. Evaluation of our method on the *Waterbirds* dataset. We observe the correlation between class ‘waterbird’ and water background (mostly blue, left) and class ‘landbird’ and land background (mostly dark, right).

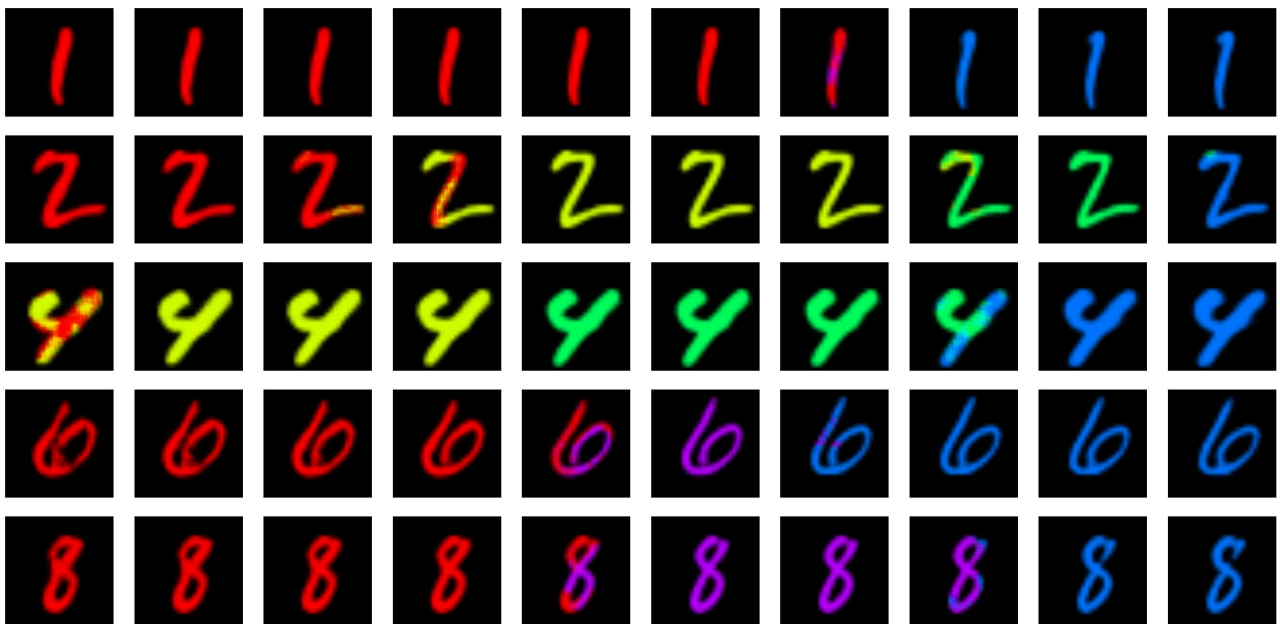


Figure 10. Evaluation of our method on the *Colored MNIST* dataset. The spurious correlation between colors and digits becomes evident with latent space traversal. The minimum values encode the colors red (left) while the maximum values encode the color blue (right).